EUROPEAN SYNCHROTRON RADIATION FACILITY

INSTALLATION EUROPEENNE DE RAYONNEMENT SYNCHROTRON

Experiment Report Form

The double page inside this form is to be filled in by all users or groups of users who have had access to beam time for measurements at the ESRF.

Once completed, the report should be submitted electronically to the User Office via the User Portal:
https://wwws.esrf.fr/misapps/SMISWebClient/protected/welcome.do

Deadlines for submission of Experimental Reports

Experimental reports must be submitted within the period of 3 months after the end of the experiment.

Experiment Report supporting a new proposal ("relevant report")

If you are submitting a proposal for a new project, or to continue a project for which you have previously been allocated beam time, you must submit a report on each of your previous measurement(s):

- even on those carried out close to the proposal submission deadline (it can be a *"preliminary report"),*
- even for experiments whose scientific area is different form the scientific area of the new proposal,
- carried out on CRG beamlines.

You must then register the report(s) as "relevant report(s)" in the new application form for beam time.

Deadlines for submitting a report supporting a new proposal

- 1st March Proposal Round - **5th March**
- 10th September Proposal Round - **13th September**

The Review Committees reserve the right to reject new proposals from groups who have not reported on the use of beam time allocated previously.

Reports on experiments relating to long term projects

Proposers awarded beam time for a long term project are required to submit an interim report at the end of each year, irrespective of the number of shifts of beam time they have used.

Published papers

All users must give proper credit to ESRF staff members and proper mention to ESRF facilities which were essential for the results described in any ensuing publication. Further, they are obliged to send to the Joint ESRF/ ILL library the complete reference and the abstract of all papers appearing in print, and resulting from the use of the ESRF.

Should you wish to make more general comments on the experiment, please note them on the User Evaluation Form, and send both the Report and the Evaluation Form to the User Office.

Instructions for preparing your Report

- fill in a separate form for each project or series of measurements.
- type your report in English.
- include the experiment number to which the report refers.
- make sure that the text, tables and figures fit into the space available.
- if your work is published or is in press, you may prefer to paste in the abstract, and add full reference details. If the abstract is in a language other than English, please include an English translation.

ESRF	**Experiment title:** X-ray phase tomography with Unified Modulated Pattern Analysis	**Experiment number**: MI-1306
Beamline:	**Date of experiment**: from: 20.10.2017 to: 22.10.2017	**Date of report**: 28.02.2019
Shifts:	**Local contact(s)**: Margie Olbinado, Lukas Helfen	*Received at ESRF:*

Names and affiliations of applicants (* indicates experimentalists):

Marie-Christine Zdora, University of Southampton (formerly: University College London and Diamond Light Source)
Irene Zanette, University of Southampton (formerly: Diamond Light Source)
Pierre Thibault, University of Southampton and Diamond Light Source
Hans Deyhle, Diamond Light Source (formerly: University of Southampton)
Joan Vila-Comamala, ETH Zurich

Report:

Scientific background:

Revealing the internal structure of biomedical samples requires imaging methods with high spatial resolution and high contrast for soft tissue, ideally capable of providing undistorted three-dimensional (3D) information from hydrated specimens. To date, conventional histology is the biomedical standard. It consists in using a light microscope to image thin slices of a specimen, which were beforehand embedded in a hard matrix and stained. Combining two-dimensional (2D) serial sections into a 3D volume is possible but time-consuming and often hindered by artefacts occurring during tissue preparation and sectioning [Ourselin et al., 2001; Pichat et al., 2018]. Moreover, conventional histology is unable to provide unbiased isotropic sampling, essential for accurate and precise volumetric analysis, and is associated with sample shrinkage due to the required dehydration step.
A suitable alternative to histology for non-destructive volumetric imaging at isotropic spatial resolution is the use of X-ray micro computed tomography (microCT) [Stock, 2008]. However, for X-ray absorption-based microCT, contrast is often too low for biomedical applications and contrast agents are required for soft-tissue discrimination [Metscher, 2009a,b; Pauwels et al., 2013; Martins de S. e Silva et al., 2015; Shearer et al., 2016; Missbach-Guentner et al., 2018; Busse et al., 2018; Müller et al., 2018], which lead to alterations in tissue structure and are often incompatible with follow-up imaging techniques.
It has been shown that X-ray phase-contrast imaging methods [Wilkins et al., 2014] can provide much better contrast for biomedical samples without the need to contrast agents [Töpperwien et al., 2018; Khimchenko et al., 2018; Wu et al., 2009; Shirai et al., 2014; Zanette et al., 2013; Velroyen et al., 2014]. However, existing methods are typically limited by elaborate experimental setups and other constraints on the nature and size of the sample. X-ray speckle-based imaging (SBI) [Morgan et al., 2012; Berujon et al., 2012; Zdora, 2018] does not impose these restrictions and benefits from a simple experimental setup that can be applied to a wide range of samples.
In this experiment, we explored the potential of X-ray phase tomography based on SBI for biomedical imaging of unstained and hydrated animal tissue.

Experimental procedure:

We used the U13 single-harmonic undulator (gap: 12.0 mm) with additional filtering by the 1.4 mm-thick diamond attenuator and 5.6 mm aluminium to obtain an X-ray beam with a narrow energy spectrum with a peak energy of approximately 26.3 keV. The experimental setup is shown in Fig. 1(a). The only addition to the standard X-ray tomography apparatus was a piece of abrasive paper used as a phase-modulating diffuser, which was fixed on translational stages for stepping in the plane transverse to the beam direction. The near-field speckle pattern created by scattering and interference of X-rays from the diffuser particles can be seen in Fig. 1(b) and in more detail in Fig. 1(c). The sample was mounted on a tomographic stage located d_1 = 72.5 cm downstream of the diffuser. Reference images (without the specimen) and sample images (with the specimen) were acquired at N = 20 different transverse positions of the diffuser. The resulting interference patterns were recorded by a detection system placed d_2 = 65.0 cm downstream of the sample. It consisted of a pco.edge 5.5 sCMOS camera coupled to a 2.1× magnification optics system, comprising two Hasselblad lenses in tandem configuration with a numerical aperture of 0.17 and a scintillation screen (250 µm-thick cerium-doped LuAG:Ce). The effective pixel size of this system was p_{eff} = 3.1 µm. The exposure time for each recorded frame was 50 ms. Acquisition of the sample images was performed in tomographic mode with 2401 projections over 180 degrees of sample rotation, which was repeated for each of the 20 diffuser positions. A set of 20 reference images was recorded before each of the tomographies and 20 dark images were taken prior to the entire scan. The scanning of various whole mouse organs (kidney, brain, testicle) was performed in two height steps with a vertical overlap of 143 pixels. Image reconstruction was performed separately for both height steps and subsequently the two phase volumes were registered and concatenated. The total scan time for the two height steps was approximately 1.5 hours.

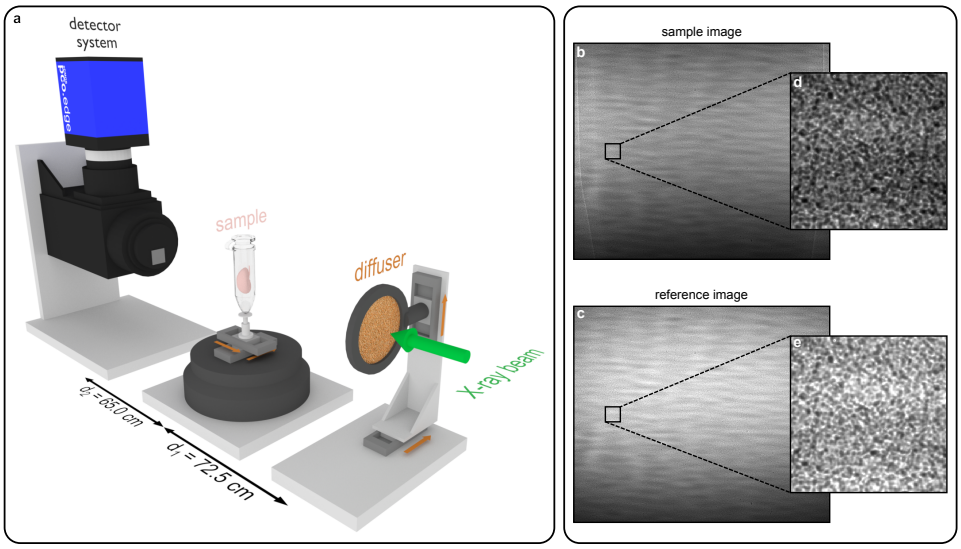

Figure 1: (a) Experimental setup for SBI phase tomography at ID19. (b),(d) Example of a sample speckle pattern and (c),(e) a reference speckle pattern.

Data analysis:

The reconstruction of the 3D phase volume was performed in several steps. First, all acquired frames were corrected for the dark current by subtracting the average dark image. Then, the differential phase signals in the horizontal and the vertical directions were reconstructed from the dark-current corrected sample and reference images recorded at the different diffuser positions. This was done for each projection of the tomography scan by applying the unified modulated pattern analysis (UMPA) approach [Zdora et al., 2017]. Although the UMPA formalism allows for multimodal signal retrieval, here the focus is on the phase-shifting properties of the specimen, which can be observed as a displacement of the speckle pattern that can be converted to the X-ray refraction angle and differential phase signal. From the differential phase signals, the phase shift images were retrieved using a Fourier phase-integration routine, combining the horizontal and vertical differential phase information [Morgan et al., 2012; Kottler et al., 2007].

The tomographic reconstruction was performed by applying a conventional filtered back-projection algorithm [Kak and Slaney, 2001] using the Python-based pyCT processing package developed by the Chair of Biomedical Physics (E17) at Technical University Munich, Germany. To reduce ring artefacts in the tomographic slices originating mainly from scintillator defects and noise, a low-pass Butterworth filter was applied to the sinogram of each slice prior to the filtered back-projection step. All of the above procedures were performed for each of the two height steps separately and finally the two volumes were concatenated.

Results:

Phase tomograms of different biomedical samples were acquired, including a mouse kidney, mouse brain and mouse testicle. In the following, some of the results obtained for the mouse kidney are presented.

Differential phase projections:

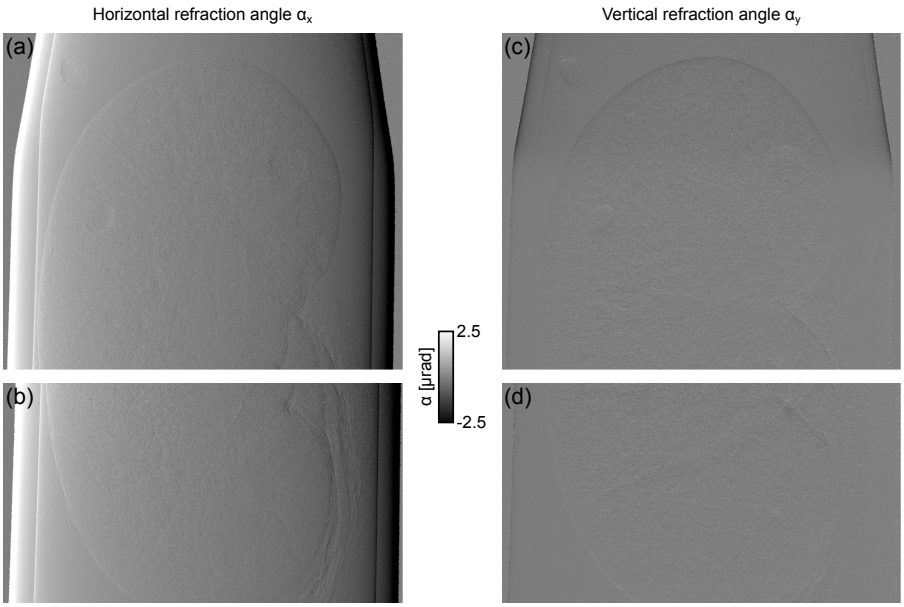

The first step in the analysis is the reconstruction of the phase-contrast signal for all of the projections recorded at different viewing angles of the sample. An example is presented in Fig. 2(a) and 2(b), showing the horizontal and vertical differential phase signal of the mouse kidney (in a plastic tube), respectively, for both of the separate tomography scans acquired for the two different height steps. The outlines of the kidney in the plastic tube can be observed, but only little detail of the inner structure of the sample is visible.

Figure 2: Differential phase projections of the mouse kidney for the two height steps. (a), (b) Horizontal and (c), (d) vertical refraction angle.

Phase tomogram:

The 3D inner structure of the unstained and fully hydrated kidney is visualised in the phase tomogram enabling non-destructive virtual histology and virtual slicing along any arbitrary plane, see Fig. 3. The micro-structural detail of the hydrated kidney tissue can be observed in the phase tomogram slice, matching that seen by conventional histology (H&E stain), performed on the same specimen after X-ray imaging. The phase volume slices are presented in histology-like false-colours for better visual comparison. (Note that the colours for the virtual phase volume slices were assigned based on tissue density, while conventional histology stains selectively attach to certain types of tissue structures.)

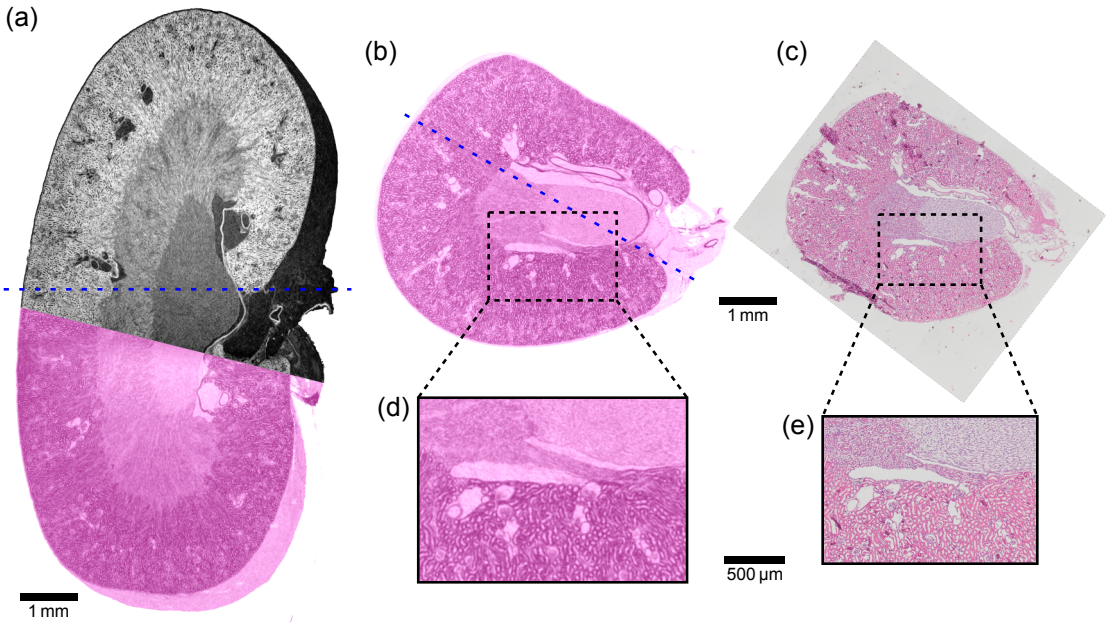

Figure 3: Virtual slices through the SBI phase tomogram of a mouse kidney validated with conventional histology. (a) Long-axis slices, (b) short-axis slice, and (c) correpsonding slices obtained by conventional histology (H&E staining). (d), (e) Regions of interest in (b) and (c), respectively, showing the same tissue microstructure.

For X-ray energies far from the absorption edges of the sample materials, the refractive index decrement δ is directly proportional to the electron density ρ_{el}. Moreover, for specimens with moderate hydrogen content, a linear relationship between ρ_{el} and the mass density ρ_m holds in good approximation. These relations allow for performing a quantitative analysis of the electron and mass density distribution within the specimen from the phase volume obtained by SBI. The high density resolution leads to excellent contrast within the kidney tissue. The spatial resolution is essentially limited by the choice of reconstruction parameters in the UMPA analysis.
The quantitative density information of the phase volume obtained by SBI can be combined with 3D information on the tissue morphology. The 3D character of the phase tomogram also provides a reliable way to perform

further structural analysis on the shape, size and distribution of some functional elements of the organ such as the blood vessel network. Retrieving this information from 2D slices, as obtained by conventional histology, can be extremely challenging.
A full analysis of the 3D structures in phase volume has been performed for the kidney and the results from this experiment are currently being prepared for submission to a peer-reviewed journal.

Conclusions and outlook:

In this experiment, we have shown that SBI phase tomography is a promising candidate for non-destructive imaging of biomedical soft tissues with high sensitivity and high spatial resolution.
SBI-based virtual histology could in the future become an invaluable tool for diagnostics and staging of diseases that lead to changes in tissue density and morphology.
As the spatial resolution and sensitivity of the measurement can be easily fine-tuned using the UMPA approach, the method can be applied to samples containing structures with a wide range of sizes and compositions, extending to fossilised matter and materials science samples.
Furthermore, although the data presented here was acquired at a synchrotron source, SBI phase tomography is being implemented at laboratory X-ray sources without major efforts or costly equipment [Zanette et al., 2014, 2015]. The optimisation of UMPA for this purpose is currently underway. This will make the method widely accessible and suitable for advanced high-throughput clinical and research applications.

References:

S. Berujon, H. Wang, and K. Sawhney, "X-ray multimodal imaging using a random-phase object," Phys. Rev. A **86**(6), 063813 (2012).

M. Busse, M. Müller, M. A. Kimm, S. Ferstl, S. Allner, K. Achterhold, J. Herzen, and F. Pfeiffer, "Three-dimensional virtual histology enabled through cytoplasm-specific X-ray stain for microscopic and nanoscopic computed tomography," Proc. Natl. Acad. Sci. **115**(10), 2293–2298 (2018).

A. C. Kak and M. Slaney, Principles of Computerized Tomographic Imaging (Society for Industrial and Applied Mathematics, Philadelphia, PA, United States, 2001).

A. Khimchenko, C. Bikis, A. Pacureanu, S. E. Hieber, P. Thalmann, H. Deyhle, G. Schweighauser, J. Hench, S. Frank, M. Müller-Gerbl, G. Schulz, P. Cloetens, and B. Müller, "Hard X-Ray Nanoholotomography: Large-Scale, Label-Free, 3D Neuroimaging beyond Optical Limit," Adv. Sci. **5**(6), 1700694 (2018).

C. Kottler, C. David, F. Pfeiffer, and O. Bunk, "A two-directional approach for grating-based differential phase contrast-imaging using hard x-rays," Opt. Express **15**(3), 1175–1181 (2007).

J. Martins de S. e Silva, I. Zanette, P. B. Noël, M. B. Cardoso, M. A. Kimm, and F. Pfeiffer, "Three- dimensional non-destructive soft-tissue visualization with X-ray staining micro-tomography," Sci. Rep. **5**, 14088 (2015).

B. D. Metscher, "MicroCT for comparative morphology: simple staining methods allow high-contrast 3D imaging of diverse non-mineralized animal tissues," BMC Physiol. **9**(1), 11 (2009a).

B. D. Metscher, "MicroCT for developmental biology: A versatile tool for high-contrast 3D imaging at histological resolutions," Dev. Dyn. **238**(3), 632–640 (2009b).

J. Missbach-Guentner, D. Pinkert-Leetsch, C. Dullin, R. Ufartes, D. Hornung, B. Tampe, M. Zeisberg, and F. Alves, "3D virtual histology of murine kidneys – high resolution visualization of pathological alterations by micro computed tomography," Sci. Rep. **8**(1), 1407 (2018).

K. S. Morgan, D. M. Paganin, and K. K. W. Siu, "X-ray phase imaging with a paper analyzer," Appl. Phys. Lett. **100**(12), 124102 (2012).

M. Müller, M. A. Kimm, S. Ferstl, F. Pfeiffer, and M. Busse, "Nucleus-specific X-ray stain for 3D virtual histology," Sci. Rep. **8**(1), 17855 (2018).

S. Ourselin, A. Roche, G. Subsol, X. Pennec, and N. Ayache, "Reconstructing a 3D structure from serial histological sections," Image Vis. Comput. **19**(1), 25–31 (2001).

E. Pauwels, D. van Loo, P. Cornillie, L. Brabant, and L. van Hoorebeke, "An exploratory study of contrast agents for soft tissue visualization by means of high resolution X-ray computed tomography imaging," J. Microsc. **250**(1), 21–31 (2013).

J. Pichat, J. E. Iglesias, T. Yousry, S. Ourselin, and M. Modat, "A Survey of Methods for 3D Histology Reconstruction," Med. Image Anal. **46**, 73–105 (2018).

T. Shearer, R. S. Bradley, L. A. Hidalgo-Bastida, M. J. Sherratt, and S. H. Cartmell, "Three-dimensional visualisation of soft biological structures by X-ray computed micro-tomography," J. Cell Sci. **129**(13), 2483–2492 (2016).

R. Shirai, T. Kunii, A. Yoneyama, T. Ooizumi, H. Maruyama, T.-T. Lwin, K. Hyodo, and T. Takeda, "Enhanced renal image contrast by ethanol fixation in phase-contrast X-ray computed tomography," J. Synchrotron Rad. **21**(4), 795–800 (2014).

S. R. Stock, Microcomputed Tomography: Methodology and Applications (CRC Press, Boca Raton, FL, United States, 2008).

M. Töpperwien, F. van der Meer, C. Stadelmann, and T. Salditt, "Three-dimensional virtual histology of human cerebellum by X-ray phase-contrast tomography," Proc. Natl. Acad. Sci. **115**(27), 6940–6945 (2018).

A. Velroyen, M. Bech, I. Zanette, J. Schwarz, A. Rack, C. Tympner, T. Herrler, C. Staab-Weijnitz, M. Braunagel, M. Reiser, F. Bamberg, F. Pfeiffer, and M. Notohamiprodjo, "X-Ray Phase- Contrast Tomography of Renal Ischemia-Reperfusion Damage," PLoS ONE **9**(10), e109562 (2014).

S. W. Wilkins, Y. I. Nesterets, T. E. Gureyev, S. C. Mayo, A. Pogany, and A. W. Stevenson, "On the evolution and relative merits of hard X-ray phase-contrast imaging methods," Philos. Trans. Royal Soc. A **372**(2010), 20130021 (2014).

J. Wu, T. Takeda, T. T. Lwin, A. Momose, N. Sunaguchi, T. Fukami, T. Yuasa, and T. Akatsuka, "Imaging renal structures by X-ray phase-contrast microtomography," Kidney Int. **75**(9), 945– 951 (2009).

I. Zanette, T. Weitkamp, G. Le Duc, and F. Pfeiffer, "X-ray grating-based phase tomography for 3D histology," RSC Adv. **3**(43), 19816–19819 (2013).

I. Zanette, T. Zhou, A. Burvall, U. Lundström, D. H. Larsson, M.-C. Zdora, P. Thibault, F. Pfeiffer, and H. M. Hertz, "Speckle-Based X-Ray Phase-Contrast and Dark-Field Imaging with a Laboratory Source," Phys. Rev. Lett. **112**(25), 253903 (2014).

I. Zanette, M.-C. Zdora, T. Zhou, A. Burvall, D. H. Larsson, P. Thibault, H. M. Hertz, and F. Pfeiffer, "X-ray microtomography using correlation of near-field speckles for material characterization," Proc. Natl. Acad. Sci. U.S.A. **112**(41), 12569–12573 (2015).

M.-C. Zdora, P. Thibault, T. Zhou, F. J. Koch, J. Romell, S. Sala, A. Last, C. Rau, and I. Zanette, "X-ray Phase-Contrast Imaging and Metrology through Unified Modulated Pattern Analysis," Phys. Rev. Lett. **118**(20), 203903 (2017).

M.-C. Zdora, "State of the Art of X-ray Speckle-Based Phase-Contrast and Dark-Field Imaging," J. Imaging **4**(5), 60 (2018).